Journal of Biochemistry and Biophysics

Volume 3 | Issue 1

Research Article Open Access

Homology Modelled Structure of Glutaredoxin 2 from *Chlamydomonas reinhardtii*

Yogesha M[1], Saini V[2], Mehta S[2], Abdul Salam AA[3], Chidangil S[1] and D'Souza JS[*1,2]

[1]Centre of Excellence for Biophotonics, Department of Atomic and Molecular Physics, Manipal Academy of Higher Education, Manipal– 576104, Karnataka, India

[2]School of Biological Sciences, UM-DAE Centre for Excellence in Basic Sciences, Kalina campus, Santacruz (E), Mumbai – 400098

[3]Department of Atomic and Molecular Physics, Centre for Applied Nanosciences, Manipal Academy of Higher Education, Manipal – 576104, Karnataka, India

[*]**Corresponding author:** D'Souza JS**,** Department of Atomic and Molecular Physics, Centre for Applied Nanosciences, Manipal Academy of Higher Education, Manipal – 576104, Karnataka, India, Tel: +91-9820770314, E-mail: jacinta@cbs.ac.in

Received Date: April 24, 2021 **Accepted Date:** May 26, 2021 **Published Date:** May 28, 2021

Citation: Yogesha M, Saini V, Mehta S, Abdul Salam AA, Chidangil S, et al. (2021) Homology Modelled Structure of Glutaredoxin 2 from *Chlamydomonas reinhardtii*. J Biochem Biophy 3(1): 102

Abstract

Different types of Glutaredoxins (GRXs) that play a major role in cellular anti-oxidative reactions have been studied for their structure and function from various organisms. Glutathione (GSH), an anti-oxidant with several medical benefits, binds to GRXs. This work has structurally characterized GRX2 from *C. reinhardtii* (CrGRX2) using biophysical, molecular modelling, and isothermal titration calorimetry (ITC) techniques. CrGRX2 adopts the classical GRX-Trx fold consisting of five β-strands surrounded by four α-helices that bind to GSH with moderate strength through a cysteine residue. The residues involved in the interaction closely match with those observed for *E. coli* and human counterparts, indicating that the cellular GSH-GRXs antioxidant system is highly conserved.

Keywords: Glutaredoxin-2; *Chlamydomonas*; Raman Spectroscopy; FTIR Spectroscopy; CD Spectroscopy; Molecular Modelling

Introduction

Abiotic stress brings about an increase in the cellular Reactive Oxygen Species (ROS) thereby causing oxidative damage. Cellular redox potential is the most distinctive feature wherein ROS can tilt the propensity of the system to either gain or lose electrons. Here, proteins that contain cysteine residues are essential as they are involved in several oxidation/reduction reactions making them an essential part of the antioxidant defence system. Glutathione (GSH; γ-glutamyl-cysteinyl-glycine), a low molecular weight thiol compound also forms a very important part of this system and detoxifies ROS directly or indirectly [1,2]. Additionally, Glutaredoxins (GRXs; 9-15 kDa) are one such kind of thiol-disulphide-oxidoreductases that belong to the thioredoxin (TRX) fold super-family, receive electrons from ribonucleotide-reductase, and reduce disulphide bonds. The reversible formation of mixed disulphide bonds between GSH and cysteine residues of proteins is known as Glutathionylation; the reverse reaction is mainly catalysed by GRXs [3-6]. The GRX system was originally discovered in a Trx1-knockout *E. coli* mutant as a dithiol hydrogen donor for ribonucleotide-reductase [7]. Both, TRXs and GRXs regulate the redox status of a cell and modulate the structure and activity of several downstream substrates. Despite low sequence similarity, TRX super-family members share a common structural motif (TRX-fold) consisting of three α-helices surrounding central four-stranded β-sheets and a CXXC active site motif essential for redox activity, a feature for interaction with cysteine-containing substrates [7]. Based on phylogenetic analysis, domain structure, and active site, GRXs are classified as dithiol GRX-containing CPYC (Class I); monothiol GRX-containing CGFS (Class II), and CC types (Class III). An N-terminus cysteine residue present on monothiol GRXs reduces the mixed disulphide between GSH and the target. This nucleophilic attack gives rise to GRX-SSG (intermediate product), later restored by GSH. In the case of dithiol GRXs, two cysteine moieties present in the active site form an intermolecular disulphide bond among themselves [8]. For the reduction of protein disulphides, both the cysteine moieties present in the active site are necessary. The disulphide bond of the target protein is attacked by thiolate resulting in the formation of the GRX-target complex and intramolecular disulphide bonds between the active site cysteine moieties, later restored by GSH, NADPH, and glutathione reductase [9]. Chronologically speaking, Class I GRXs, the most widespread, were first discovered in *E. coli* [7], now known to be present in all organisms, was followed in the late 1990s by the Class II found chiefly in eukaryotes and most proteobacteria. On the other hand, Class III is specific to the plant kingdom. The post-genome sequencing era has led to the identification of three more classes of GRXs, particularly from photosynthetic organisms [10]. The fourth class (Class IV) contains the N-terminal GRX domain, in addition to two domains of unknown functions. Two more GRX classes (Class V and VI), of which Class V is seen in some bacteria, while Class VI is specific to cyanobacteria contain either an N-terminal domain of unknown function or a C-terminal transmembrane portion, respectively [10]. Lower eukaryotes such as *Chlamydomonas reinhardtii* have fewer numbers of GRXs as compared to *Arabidopsis*, the latter genome having 31 Grx genes. The proteins encoding these genes belong to three types, 21 are of the typical land plant CC-types; the rest of them belong to the conventional prokaryotic and eukaryotic, CPYC and CGFS types [11]. The genome of *C. reinhardtii* harbours two cytosolic CPYC-types (GRX1–2) and four organellar CGFS-types (GRX3–6) [5,6].

Several three-dimensional structures of GRX2 from *E. coli* (PDB Id: 4KX4); [12] human (PDB Ids: 2FLS and 1JHB) [13], *Saccharomyces cerevisiae* (PDB Id: 3CTF) [14], *Clostridium oremlandii* [15,16] determined either in the reduced/oxidized forms through X-ray crystallography/NMR spectroscopy are available at Protein Data Bank (PDB). Grx2 proteins belong to the TRX family proteins. The TRX-fold has a common structural motif, with a classical α/β-fold. The TRX-fold generally consists of four-stranded antiparallel β sheets sandwiched between three α helices. The β strand topology is 2134, and the 3rd β strand is antiparallel to others. In higher organisms, like CrGRX2, the structural motif may have additional α-helices or β-sheets [17,18]. Biochemical characterization of CrGRX2 provided insights into kinetics and deglutathionylation reactions [6]. In addition, the TRX-fold and TRXs as well as GRXs being highly conserved, these have served as subjects of evolutionary studies, especially in the context of redox biology [19]. The current study structurally characterizes CrGRX2 through Raman, FTIR, CD spectroscopy, and *in silico* molecular modelling, along with identifying the critical residues involved in the GSH binding. Further, the exchange reaction between the oxidized GSH and reduced CrGRX2 leading to the formation of the mixed disulfide was monitored by ITC; the measured binding constant compares well with earlier studies on yeast, indicating that recombinant CrGRX2 protein whose secondary structure elucidated herein is completely reliable. The interaction is largely enthalpy-driven with a large entropy penalty. The thermodynamic parameters indicate the similarity between CrGRX2 and those from other organisms.

Materials and Methods

Isolation, Over-expression, and Purification

Chlamydomonas reinhardtii Grx2 gene (NCBI Reference Sequence: XM_001693949.1 for mRNA, Gen ID:5719651, Protein_id: XP_001694001.1; https://www.uniprot.org/uniprot/A8IYH1, of 330 bp) cloned between *NdeI and Bam*HI RE sites of pET duet vector was a gift from Stephane Lemaire [6]. The 6XHis-tagged recombinant CrGRX2 over-expressed in *E. coli* (BL21DE3) was purified to homogeneity using Ni-NTA affinity chromatography [20]. Purified protein was dialyzed, checked for the 6XHis-tag, and mass determined with Bruker UltrafleXtreme MALDI-TOF instrument (TIFR, Mumbai, India).

Biophysical techniques (Raman spectroscopy and FTIR spectroscopy)

Pure, lyophilized powder (1-2 mg) of the recombinant CrGRX2 protein was used for obtaining Raman spectra from a locally assembled micro-Raman spectrometer having Horiba Jobin-Yuon Spectrograph (iHR-320) coupled with an inverted microscope (Nikon Eclipse Ti-U, Japan). A diode laser source (Starbright Diode Laser, Torsana Laser Tech, Denmark, 785 nm) illuminated the sample sandwiched between quartz cover-slip and borosilicate glass slide. The laser beam was focussed and back scattered Raman radiations were collected by using a 60X microscope objective. The Raman spectra of the sample were recorded by the above mentioned spectrometer coupled with a liquid nitrogen cooled Symphony CCD detector. Thirty spectra (spectral range: 200-1800 cm^{-1}, resolution: 5 cm^{-1}, accuracy: 2 cm^{-1}, slit width: 100 μm, and laser power: 47 mW) with 5 mins of acquisition time were obtained. FTIR spectra of the purified lyophilized protein were recorded at RT by mixing with KBr to form discs. Five hundred scans with 2 cm^{-1} spectral resolution were measured using a JASCO6300 spectrometer equipped with a DLATGS detector and a standard source.

Data processing

Raman and FTIR data were processed and analysed using Origin-Pro8 (Origin Lab, Northampton, MA) and GRAMS (Grams/32, Galactic Software Inc., NH, USA) software. Raman and FTIR spectra were smoothened, base-lined averaged and normalized to an area of unity. The second derivatives of these spectra were calculated to reveal the hidden peaks using GRAMS.

Secondary structure analysis

CD spectra were measured (JASCO-CD Polarimeter J-810) in a cuvette with 1 mm path length, 190-260 nm with a bandwidth of 1 nm, and limited to 50 nm/s. The sample (0.1 mg/ml) was dialyzed (10 mM K-Phosphate buffer, pH 7.7), and the chamber was continuously flushed with N_2 gas. The resultant spectral values are expressed in units of mdeg (millidegrees). Deconvolution was performed using the online BeStSel analysis program [21] applied at 190-250 nm.

Tertiary structure prediction and validation

CrGRX2 tertiary structure was initially predicted by the *ab initio* method of the QUARK program [22]. QUARK assembles the protein structure from models of small fragments (1-20 residues) by replica-exchange Monte Carlo simulation. It requires no templates for structure prediction and is guided by an atomic-level knowledge-based force field. With five different models resulting from the output, the quality of each was assessed and validated using SWISS-MODEL web-server [23]. The server provides QMEAN [24], Z-score, and MolProbity score [25] to assess the models' quality. QMEAN provides quality estimates for the entire structure (global model) and per residue (local model) based on one single model. Z-score assesses the nativeness of the model observed comparing the high-resolution experimental structures of similar sizes. QMEAN Z-scores of ≤-4.0 indicate a low-quality model, and those around zero indicate a good-quality model. The secondary structure for the target protein sequence was predicted by DSSP [25].

The CrGRX2 model was also build using the online homology modelling server SWISS-MODEL (https://swissmodel.expasy.org/). The crystal structure of reduced GRX from *Chlorella sorokiniana* T-89 in complex with GSH (PDB ID: 4I2U, resolution 1.3 Å) was selected as a template to build a monomer model of CrGRX2. Both share sequence similarity of 58%. The monomer model with GSH was constructed with a QMEAN score of -0.11, whose model quality was assessed using MolProbity (http://molprobity.biochem.duke.edu) [26]. The server yielded a MolProbity score of 1.19, which is the 99th percentile of the best high-quality model with no Ramachandran outlier. The monomer model was further minimized using UCSF Chimera (version 1.14) with default settings [27]. The protein-ligand interaction calculations were carried out using PLIP [28], and Ligplot+ (version 2.2) (https://www.ebi.ac.uk/thornton-srv/software/LigPlus/) [28]. PyMOL (The PyMOL Molecular Graphics System, Version 2.0 Schrödinger, LLC.) and Ligplot+ were used to render the molecular interaction figures.

Isothermal titration calorimetry (ITC) and glutathione binding

Purified CrGRX2 was dialyzed at 4 °C with 30 mM Tris (pH 7.7), and150 mM NaCl, followed by 10 mM K-Phosphate buffer (pH 7.7). GSH (0.5 mM) prepared in the latter buffer was used for binding with CrGRX2 using MicroCal iTC200 (Malvern, MicroCal, Northampton, MA). All solutions were degassed, the reference cell contained a buffer, the sample cell contained the binding partner, and the ligand solution was titrated using a stirring syringe into the sample cell. The titrations were carried out at 25 °C with a stirring rate of 350 rpm. Each experiment consisted of 19 consecutive injections, each 2 µl X 0.5 mM GSH into the sample cell containing 0.05 mM GRX2 for 60 sec with an interval of 2 min between the consecutive injections. Analysis of the titration heat profiles was done using Origin8.0 software. The data were fitted with the One-Set-of-Sites model to calculate the binding constant (K), stoichiometry (N), change in enthalpy (ΔH), and change in entropy (ΔS). ΔG and ΔS were calculated from the standard thermodynamic relations:

$$\Delta G = -RT\ In\ K \qquad (1)$$

$$\Delta s = \frac{\Delta H - \Delta G}{T} \qquad (2)$$

R is the universal gas constant (8.3144 $Jmol^{-1}\ K^{-1}$), and T is the absolute temperature (297 °K).

Results and Discussion

Multiple sequence alignment and purification

Chlamydomonas reinhardtii protein sequences (GRX1-6) aligned to construct a phylogenetic tree (Figure S1) revealed clustering of CPYC and CGFS. CrGRX2 (107 aa) BLAST (Figure S2) with ~100 organisms indicated 48-76% identity with GRXs from algae, fungi, nematode, protozoans, mono- and di-cotyledenous plants (score of $3e^{-51}$ to $4e^{-26}$) with an average query cover of 85% and the conserved CPYC active site across organisms. Some conserved stretches and Glycine residues were also observed (Figure S2, filled boxes and circles). Some of these glycines (88 and 89) are predicted to be involved in interaction with GRX2 (see below). While a detailed biochemical characterization of *C. reinhardtii* GRXs has been accomplished [6], the present study uses three biophysical tools to confirm the secondary structure of the CrGRX2. The micro-Raman spectroscopy, Circular Dichroism, and FTIR spectroscopy techniques were used to establish the number of unequivocally-helices, β-sheets, and random coils in CrGRX2 and confirm the residues interacting with GSH.

6XHis-tagged recombinant CrGRX2 over-expressed in *E. coli* was purified to homogeneity using Ni-NTA affinity chromatography (Figure S3A). The purity and molecular weight (12.7 kDa) were ascertained using MALDI-TOF (Figure S3B). The tag was confirmed using Western blotting and anti-6XHis antibody probing (Figure S3A, lane 3). Like most GRXs, CrGRX2 is also a small molecular weight protein with ~77% of its linear sequence covered by the GRX domain [6,30].

Secondary structure determination using biophysical techniques

Analysis of CrGRX2 micro-Raman spectra - Amide band signatures, Amino acid signatures, C-C and C-N skeletal modes: Raman spectroscopy is a versatile scattering technique widely accepted for the characterization of biological macromolecules. The inelastically scattered light from the sample, popularly known as Raman scattered light contains rich information about molecular vibrations. The primary condition to obtain Raman scattering from a specific molecular bond is that it should undergo a polarizability change during the light (laser) matter interaction. The Raman scattered light can be recorded using dedicated spectrometers and the resulting spectrum will provide vibrational frequencies of most of the molecular bonds in the molecules. Micro-Raman spectra of proteins yield good information about the protein secondary structure. The prominent Raman frequencies observed in CrGRX2 are given in Table S1.

The Amide I band (1640-1680 cm^{-1}) is contributed by carbonyl stretching of the peptide backbone; whereas, the Amide III band (1230-1310 cm^{-1}) is contributed by in-plane N-H bending and stretching of C-N bond [31]. In the micro-Raman spectra of the CrGRX2 protein, amide I band frequencies were observed at 1653 and 1668 cm^{-1}, indicating CrGRX2 contains both α-helix and β-strand as secondary structures (Figure 1A). The amide III bands' peak frequencies observed at 1236 and 1285 cm^{-1} correspond to β-strand and α-helix, respectively. Also, the Amide III spectral region 910-950 cm^{-1} correlates with the α-helical structure of the protein [32,33]. The second derivative calculation for 1640-1680 cm^{-1} with the marked peak frequencies (1646, 1651, 1654, 1659, and 1668 cm^{-1}) confirm both α-helix and β-strand with more amount of α-helix compared to β-strand (Figure 1B). Analysis of Amide I and III bands also revealed the presence of irregular/random coils in CrGRX2 (Table S1). A 521 cm^{-1} band indicated disulphide linkage with gauche-gauche *trans* conformation between S-S linkage (Figure 1A). The para-substituted phenyl ring of tyrosine yields strong Raman signatures at 850 and 828 cm^{-1}. The phenomenon of Fermi resonance forms tyrosine doublets. An intensity ratio (0.3-2.5) of tyrosine frequencies at 850 and 828 cm^{-1} (I_{850}/I_{828}) reveals the hydrogen bonding state of the tyrosine phenoxyl group. A value of 0.3 indicates buried tyrosine (the phenolic OH group acts as a strong hydrogen bond donor) and that of ~1.25 shows exposed tyrosine (acts as both donor and acceptor). A value of 2.5 indicates tyrosine residues as strong hydrogen acceptors [32]. In CrGRX2, the tyrosine Fermi doublet appears at 825 and 850 cm^{-1} and an I_{850}/I_{828} ratio of ~1.0, indicates that tyrosine is exposed and acts as both donor and acceptor. An intense aromatic residue band associated with phenylalanine is observed at 999 and 1177 cm^{-1} (Figure 1). Non-aromatic residues exhibit low polarizability of their aliphatic side chains and thus yield weak Raman signatures, their correct interpretation being critical in the protein structure [43]. In CrGRX2, the peak frequencies at 721, 894, 902, 1060, and 1457 are likely associated with methionine, lysine, alanine, arginine, or lysine and alanine.

Qualitative and Quantitative analysis by FTIR coupled with PLSR: Complementary to Raman technique, Infrared Absorption spectroscopy can also provide vibrational information of molecules present in samples. Infrared Absorption of radiation occurs when the molecular bond undergoing IR absorption is associated with a permanent dipole moment. Fourier transform infrared (FTIR) spectroscopy is the absorption spectroscopy technique used to study the infrared absorption spectrum of samples. This technique measures high-resolution vibrational spectrum of samples over a wide range, usually between 400 and 4000 cm^{-1} for mid-IR region wavelength. The absorption of light in broad range can be recorded simultaneously and this process can be repeated many times resulting into a very high signal-to-noise ratio for a specific scanning time. FTIR spectroscopy is a popular technique used to investigate the secondary structure of the proteins.

The mean FTIR spectrum of CrGRX2 was obtained by averaging twenty spectra (Figure 1C). Spectral regions from 1600-1690 cm^{-1} (Amide I) arise from C=O group stretching vibrations, C_{α}-C-N deformation, and C-N out-phase stretching vibrations, while those from 1480-1575 cm^{-1} (Amide II) occur due to a mixture of several vibrations of peptide bonds. N-H in-plane bending vibration is the major contributing vibration for the Amide II band [43]. The strong band around 1648-1660 cm^{-1} is assigned to α-helices, while the intense band around 1621-1641 cm^{-1} is assigned to β-sheets. Random coils and β-turns are assigned to 1640-1650 cm^{-1} and 1662-1684 cm^{-1} respectively [44]. An intense band around 1650 cm^{-1} in the FTIR spectrum of CrGRX2 suggested that the protein is mainly α-helical in nature.

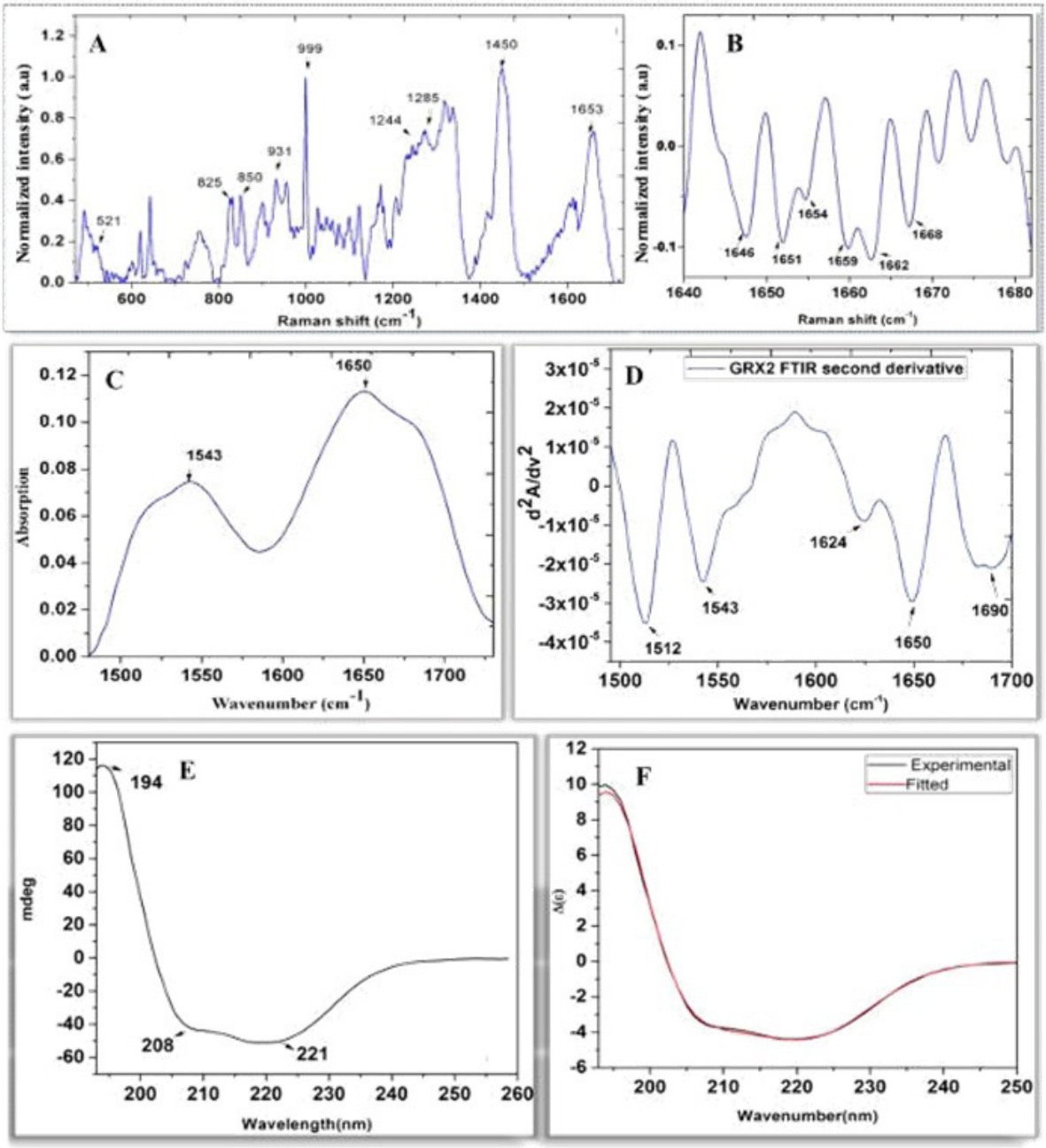

Figure 1: (A) Raman Spectra of CrGRX2 recorded in the spectral region of 500-1700 cm^{-1}; **(B)** Amide I band (1640-1680 cm^{-1}) ; **(C)** Normalized mean FTIR spectra, Min-Max normalized averaged FTIR spectra and; **(D)** Second derivative of amide I and amide II regions (1500–1700 cm^{-1}); **(E)** Far-UV CD spectra in the 190-260 nm range (mdeg); **(F)** Comparison plot of experimental (CD) and calculated spectra through the BeStSel server (Delta Epsilon, Δε). Note the goodness of fit using Raman and FTIR methods

Amide I band is extensively used to study protein secondary structure, aggregation, stability, unfolding, and folding properties. Since the amide I band's complexity arises from unresolved components, it becomes difficult to estimate the secondary structure of proteins [45]. To unravel or resolve the overlapped amide I bands, the second derivative of the band was calculated (Figure 1C). The absorption spectrum shows an amide I band maximum at 1650 cm^{-1}. The second derivative spectrum (Figure 1C) affirms the presence of a number of peaks, such as 1624 and 1690 cm^{-1} assigned to β-sheets, and 1650 cm^{-1} can be assigned to α-helix. Additional bands that appeared in the amide II region, such as 1543 and 1512 cm^{-1}, can be assigned to α-helix and tyrosine, respectively [43-45]. The FTIR spectra of standard proteins were mixed with the matrix for the spectral regions from 1500-1700 cm^{-1} (Amide I and II regions combined) followed by partial least square (PLS) modelling. The second derivative of the CrGRX2 (Figure 1C) for 1500-1700 cm^{-1} was employed to quantify the secondary structure. As per PLSR calculations, CrGRX2 is ~34% α-helical, 14% β-sheets, 14% β-turns, and 38% of other secondary structures; and the prediction deviation for the structure is 0.9-1 (Table 1).

Fraction of each secondary structure (%)						RMSD	NRMSD
H1	H2	APB	PB	Turn	Other		
20	9.8	4.0	9.0	14	44	0.177	0.012
30		13					

Table 1: Secondary structure calculated from BeStSel web-server

Secondary structure quantification using Circular Dichroism followed by BeStSel analysis: Circular dichroism (CD) spectroscopy is a standard absorption technique to study secondary structures present in macromolecules. It is a form of light absorption spectroscopy that measures the difference in absorbance of right- and left-circularly polarized light by a sample. The spectral signatures pertaining to the secondary structures for alpha helix, parallel and antiparallel beta sheet, turn, and others can be analyzed in the 180 -260nm spectral region of the CD spectra. The CD results were *in sync* with the Raman and FTIR spectral analysis of CrGRX2. The Far-UV CD (190–250 nm) spectra showed two minimum peaks at 208 and 221 nm and one maximum peak at 194 nm (Figure 1E-F), indicating α-helix as its major secondary structure. Quantification (Figure 1E-F) using BeStSel revealed ~30% of α-helix. Of these, the regular helix (H1) was 20%, while the shorter (H2) was 9.8%. At the same time, ~4% of antiparallel β-sheets, 9% parallel β-sheets, 14% of β-turns, and 44% of unordered structures were present in the protein (Table 1). The NRMSD value was as low as 0.012, indicating the reliability of the predicted values. These results are in good agreement with FTIR quantification. Overlapped experimental and calculated CD spectra (Figure 1F) show goodness-of-fit obtained using both these methods confirming the modality used. The work was further extended to recognize the fold of the protein using Class, Architecture, Topology, Homology (CATH) classification provided by the BeStSel web-server [46]. Based on the input CD data supplied by the user BeStSel segregate, twenty closest structures were identified considering the Euclidean distance by searching throughout the PDB. The resultant structures are listed out with CATH classification. Weighted K-nearest neighbors (WKNN) search based on CD spectra of CrGRX2 CATH analysis revealed that CrGRX2 belongs to α-β class with two or three-layer sandwich architecture. The topology and homology of the CrGRX2 protein were identified to be 'Glutaredoxin' with CATH identification numbers (3.40.30 and 3.40.30.10). This confirmed the native state of CrGRX2 having Glutaredoxin fold.

CrGRX2 tertiary structure

The CrGRX2 model has classical Grx/Trx-fold with a core of four β-strands flanked by five α-helices. Helices α1 and α3 are on one side of the β-strands; α2, α4, and α5 are on the other side. α4 is almost perpendicular to α5 with only one residue (Gly99) between them. The three β-strands (β1, β3, and β4) are parallel to β*2* (Figure 2C). Four residues (Gln64, Val76, Gly89, Asp90) make six-strong hydrogen bonds with GSH. Apart from the hydrogen bonds, Lys28 makes a salt bridge with the carboxylate of GSH. Besides Cys31, Tyr33 and Pro77 are involved in hydrophobic interactions (Figure 2D-E). Cys31, a part of the $_{31}$CPYC$_{34}$ active site, is within 3.45 Å from the sulfur atom of GSH, and the interaction energy is -4.6 kcal/mol (Table 2). The predicted CrGRX domain, GSH-interacting residues, and catalytic site were compared with the human (PDB Id:2FLS) and *E. coli* (PDB id:4KX4) GRX2 structures crystallized with GSH (Table 2, and Figure 2F-G). The results suggest that all the ten residues of CrGRX2 (Lys28, Cys31, Tyr33, Gln64, Ser75, Val76, Pro77, Gly88, Gly89, and Asp90) interacting with GSH (Table 2, Figure 2F) are conserved and have similar interactions as HsGRX2 (Figure 2G) and EcGRX2 (Figure 2H) structures. Out of 10 residues, except Ser75 (Thr80 for HsGRX2), Gly89 (Ala94 for HsGRX2), and Asp90 (Thr95 for HsGRX2), the remaining seven residues of CrGRX2 are conserved with HsGRX2 (Table 2). In comparison with EcGRX2, four residues of CrGRX2 Cys31 (Cys9 of EcGRX2), Tyr33 (Tyr11 of EcGRX2), Val76 (Val48 of EcGRX2), and Pro77 (Pro49 of EcGRX2) are conserved. Interestingly, the Asp90 in CrGRX2 is making stronger hydrogen bonds with GSH than the human (Thr95) and *E. coli* (Ser62) GRX2 structural models. These results are congruent with those on GRX2 from *Chlorella sorokiniana* T-89 and *Homo sapiens* [47,48]. The human GRX-2 (PDB id: 2FLS (monomer) and PDB id: 2HT9 (dimer) has four cysteine residues (Cys28, Cys37, Cys40, and Cys113). In which Cys37-Cys40, Cys28-Cys113 pairs are in close proximity to each other. The Cys37-Cys40 pair is conserved and involved in catalysis, whereas the second pair Cys28-Cys113 forms a disulfide and is approximately 23.0 Å away from the catalytic pair [49]. In CrGRX2 three cysteine residues (Cys31, Cys34, and Cys60) are present. Superposition of the HsGRX2 with CrGRX2 yields an RMSD of 0.684 Å.

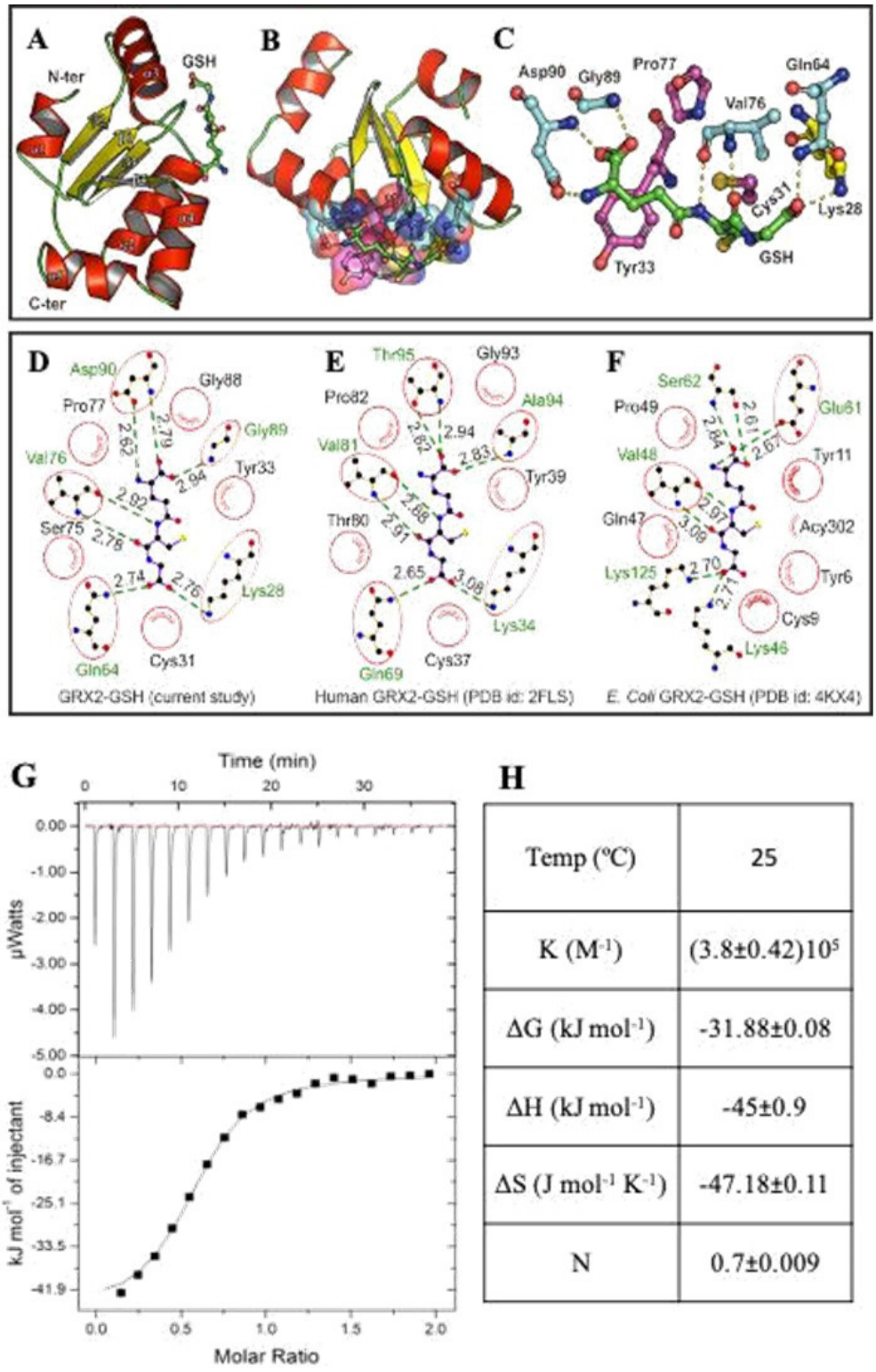

Temp (°C)	25
K (M^{-1})	$(3.8\pm0.42)10^5$
ΔG (kJ mol^{-1})	-31.88±0.08
ΔH (kJ mol^{-1})	-45±0.9
ΔS (J mol^{-1} K^{-1})	-47.18±0.11
N	0.7±0.009

Figure 2: Interaction between CrGRX2 and GSH (A) Secondary structural units of CrGRX2 model N-α1-β1-α2-β2-α3-β3-β4-α4-α5-C are marked. The helices are red-coloured, and strands are yellow. GSH is shown in the ball-and-stick model; **(B)** The interaction of CrGRX2 with GSH with selected residues Substitute was with is shown on the surface model; **(C)** Closer view of CrGRX2-GSH interactions; residues that make hydrogen bonds, hydrophobic contacts, and salt-bridge are cyan (carbon atoms), magenta, and yellow. The hydrogen bond and salt bridge interactions are shown in dotted lines; **(D)** CrGrx2-GSH interactions using Ligplot within 4.0 Å proximity of GSH. (Hydrogen bonds, green dotted lines; Hydrophobic contacts, spokes radiating towards the GSH atoms); **(E)** HsGrx2 with GSH interactions retrieved from PDB id: 2FLS; and **(F)** EcGrx2 with GSH interactions retrieved from PDB id: 4KX4. Common residues of GRX2 making interactions with GSH in all cases are marked within circles. **(G)** ITC thermogram (upper panel) and; **(H)** isotherm (lower panel) are depicted

Protein Amino acid (Donor) of CrGRX2	Ligand atom	Donor-H … Ligand distance (Å)	Donor – Ligand distance (Å)	Donor Angle (0)	Equivalent residues of Human/E. coli Grx2
Hydrogen bonds					
Gln64	O (CO2)	1.72	2.74	172.44	Gln69/Ala36
Val76	O2	1.98	2.92	153.08	Val81/Val48
Val76	O2	1.83	2.78	153.48	Val81/Val48
Gly89	O (CO2)	1.93	2.94	169.91	Ala94/Glu61
Asp90	O (CO2)	1.81	2.79	161.25	Thr95/Ser62
Asp90	O3	1.68	2.62	144.99	Thr95/Ser62
Hydrophobic contacts					
Cys31			3.45		Cys37/Cys9
Tyr33			3.70		Tyr39/Tyr11
Ser75			3.92		Thr80/Gln47
Pro77			3.50		Pro82/Pro49
Gly88			3.36		Gly93/Glu60
Salt Bridges					
Lys28	Carboxylate		2.76		Lys34/Tyr6

Table 2: GRX2 and GSH interaction: Summary of residues involved in the interaction of human, *E. coli* and *C. reinhardtii* GRX2s

The result shows that the CrGX2 Cys31-Cys34 pair is equivalent to the HsGRX2 Cys37-Cys40 pair and involved in GSH binding. It may be emphasized that in HsGrx2, non-active Cys residue is known to play an important role while catalysing the dithiol reaction. In CrGRX2, the Cys60 is not conserved and is approximately 14 Å away from Cys31 of CrGRX2. Thus, we do not find an equivalent non-active Cys residue/s such as Cys28-Cys113 of HsGRX2 and the role of Cys60 of CrGRX2 in catalysing dithiol reaction is yet to confirm. Further experiments are necessary to validate the role of Cys60.

Isothermal Titration Calorimetry

A thermogram for titrations of 0.5 mM GSH with 0.05 mM CrGRX2 at pH 7.4 and 25 ^{o}C was obtained (Figure 2A). Raw data for 19 consecutive injections of GSH into the protein solution was used for the integrated binding heats as a function of the [GSH]/[GRX2] molar ratio. The isotherm was fitted with the 'One-Set-of-Sites' model, and the smooth solid lines shown (Figure 2A) in the lower portion are the best fit for the experimental data. The thermodynamic parameters thus measured are an average of three independent measurements (Figure 2B). The reported enthalpy is not influenced by the buffer used for the experiment because the ionization enthalpy for the phosphate is significantly less ($\Delta H_{ionization}$=3.6 kJ/mol). The heat profiles (Figure 2A) have been corrected for the dilution effects. The negative heat of interaction indicates that the binding is exothermic with an affinity constant of the order of 10^5, suggesting moderate binding [50-52].

Both the entropy and enthalpy are negative, indicating an enthalpy-driven, unfavourable entropy reaction. The enthalpy enables us to understand the nature of the interaction (hydrogen bonding, hydrophobic and electrostatic), whereas entropy explains the freedom/restriction of the molecule upon binding [51,52]. The negative entropy is probably the result of limitation in the protein conformation besides the lost conformational, translational, and rotational freedom on binding to GSH [50]. Since ΔH=-45±0.9 kJ/mol and ΔS=-47.18±0.11 $Jmol^{-1}K^{-1}$ are negative, it indicates the formation of hydrogen bonds and *van der* Waals interactions. The interaction (K=3.8±0.42 X 10^5 M^{-1}) also supports the concept of enthalpy-entropy compensation, as enthalpy is favourable, entropy is not. Free energy, ΔG, is also negative (-31.88±0.08 kJ/mol), denoting spontaneous/exergonic and favourable for the binding [51,52]. Given these interactions, and a physiological concentration of GSH between 0.5-10 mM [53], we speculate that this interaction might operate when the ROS levels are high and the GSH concentration builds up inside cells.

Earlier reports on the biochemical characterization of *Chlamydomonas* GRXs have revealed obvious yet unique differences in the CPYC (GRX1 and GRX2) and CGFS-type (GRX3-6) GRXs, not just in their sequences, but also in their classical GRX activities [6]. GRX5 and GRX6, do not possess disulfide reductase and DHA reductase activities, poorly catalyze deglutathionylation, and use their active site and C-terminal cysteines to form intermolecular disulfide bonds. These results are consistent with those observed for GRXs from diverse sources [6,54,55, 56]. Further, the pK_a of the various activities obtained for both GRX1 and GRX2, were found to be very similar to those of human GRX1 and GRX2 [57]. It may also be noted that GRX1 and GRX2 catalyze deglutathionylation at different rates. Such a similarity is reminiscent of *Chlamydomonas*, making it an excellent model to study redox potential so as to use it for human proteins [58]. On the other hand, *Chlamydomonas* chloroplastic GRX3 is a CGFS-type GRX and has very different and unexpected biochemical properties. First, akin to CGFS-type GRX from yeast [55] and *E. coli* [54], GRX3 is not reduced by GSH, it lacks activity in the DHAR and HED assays but not in the insulin assay. It has an atypically negative redox potential of –323 ± 4 mV at pH 7.9, which is the physiological pH of the chloroplast stroma in the light. This value is much closer to the redox potentials classically reported for TRXs than GRXs [59]. The redox potential of another CGFS-type GRX, yeast mitochondrial GRX5, has been previously reported to be –175 mV [55]. This reflects the differences in the redox properties between species or between subcellular compartments. With no apparent CPCY GRX in the chloroplast, studying protein deglutathionylation with GRX3, especially with chloroplastic substrates like those belonging to the Calvin cycle, can serve as a representative study for photosynthetic organisms while investigating photosynthetic metabolism. The interplay of these GRXs in *Chlamydomonas* therefore prove to be useful towards a better understanding of how the cell adjusts its intracellular redox states operating in different metabolic pathways. In this light, any small addition in the biochemical and structural properties of these GRXs would be considered as impactful. This study has quantified secondary structural features as ~30% α-helices, 13% β-sheets, 14% β-turns, and ~44% unordered structure. The results show a α-β class of protein with the classical GRX-fold binding to GSH with moderate strength between α2-α3-α4 helices, involving a cysteine.

Declaration of interests

None

Acknowledgments

YA, SC, and JSD acknowledge grant (BT/PR3159/BRB/10/960/2011/dated23/08/2012) received from the Department of Biotechnology, India. YA received a stipend from this grant. AAAS acknowledges an intramural grant provided by the Manipal Academy of Higher Education (MAHE/DREG/PhD/IMF/2019). JSD acknowledges grx2-gene-containing plasmid gifted from Prof. Stephane Lemaire, Biologie Computationnelle et Quantitative UMR 7238 CNRS - Sorbonne Université Institut de Biologie Paris, France. JSD also acknowledges Prof. Ankona Datta for granting permission to access the MALDI-TOF instrument and Mrs. Gitanjali Dhotre for extending technical help with the MALDI-TOF spectrum (TIFR, Mumbai, India).

Supplementary

References

1. Foyer CH, Noctor G (2005) Redox homeostasis and antioxidant signaling: a metabolic interface between stress perception and physiological responses. Plant Cell 17: 1866-75.

2. Foyer CH, Noctor G (2005) Oxidant and antioxidant signaling in plants: a re-evaluation of the concept of oxidative stress in a physiological context. Plant, Cell Environ 28: 1056-71.

3. Berndt C, Lillig CH, Holmgren A (2008) Thioredoxins and glutaredoxins as facilitators of protein folding. Biochim et Biophys Acta-Molecular Cell Research 1783: 641-50.

4. Herrero E, Bellí G, Casas C (2010) Structural and functional diversity of glutaredoxins in yeast. Current Protein and Peptide Science 11: 659-68.

5. Zaffagnini M, Michelet L, Massot V, Trost P, Lemaire SD (2008) Biochemical characterization of glutaredoxins from Chlamydomonas reinhardtii reveals the unique properties of a chloroplastic CGFS-type glutaredoxin. J Biol Chem 283: 8868-76.

6. Gao X-H, Zaffagnini M, Bedhomme M, Michelet L, Cassier-Chauvat C, et al. (2010) Biochemical characterization of glutaredoxins from Chlamydomonas reinhardtii: kinetics and specificity in deglutathionylation reactions. FEBS Lett 584: 2242-8.

7. Fernandes AP, Holmgren A (2004) Glutaredoxins: glutathione-dependent redox enzymes with functions far beyond a simple thioredoxin backup system. Antioxidants and Redox Signaling 6: 63-74.

8. Begas P, Liedgens L, Moseler A, Meyer AJ, Deponte M (2017) Glutaredoxin catalysis requires two distinct glutathione interaction sites. Nat Comm 8: 14835.

9. Ströher E, Millar AH (2012) The biological roles of glutaredoxins. Biochem J 446: 333-48.

10. Couturier J, Jean-Pierre J, Rouhier N (2009) Evolution and diversity of glutaredoxins in photosynthetic organisms. Cell Mol Life Sci 66: 2539-57.

11. Ji-Yul J, Ahn JH, Schachtman DP (2018) CC-type glutaredoxins mediate plant response and signaling under nitrate starvation in Arabidopsis. BMC Plant Biology 18: 281.

12. Ye J, Venkadesh Nadar S, Li J, Rosen BP (2014) Structure of Escherichia coli Grx2 in complex with glutathione: a dual-function hybrid of glutaredoxin and glutathione S-transferase. Acta Crystallographica D: Biological Crystallography 70: 1907-13.

13. Chaohong S, Berardi M, Bushweller J (1998) The NMR solution structure of human glutaredoxin in the fully reduced form. J Mol Biol 280: 687-701.

14. Wei-Fang L, Jiang Y, Xiao-Xiao M, Yan-Bin T, Ming L, et al. (2010) Structural basis for the different activities of yeast Grx1 and Grx2. Biochim. et Biophys. Acta 1804: 1542-7.

15. Lee EH, Kim H-Y, Hwang KY (2014) The GSH- and GSSG-bound structures of glutaredoxin from Clostridium oremlandii. Arch Biochem Biophys 564: 20-5.

16. Lee K, Yeo KJ, Choi SH, Lee EH, Kim BK, et al. (2020) Monothiol and dithiol glutaredoxin-1 from Clostridium oremlandii: identification of domain-swapped structures by NMR, X-ray crystallography and HDX mass spectrometry. IUCr J 7: 1019-27.

17. Hanschmann EM, Godoy JR, Berndt C, Hudemann C, Lillig CH (2013) Thioredoxins, glutaredoxins, and peroxiredoxins--molecular mechanisms and health significance: from cofactors to antioxidants to redox signaling. Antioxid Redox Signal 19: 1539-605.

18. Atkinson HJ, Babbitt PC (2009) An Atlas of the Thioredoxin Fold Class Reveals the Complexity of Function-Enabling Adaptations. PLOS Computational Biology 5: e1000541.

19. Meyer Y, Buchanan BB, Vignols F, Reichheld J-P (2009) Thioredoxins and glutaredoxins: unifying elements in redox biology. Annu Rev Genet 43: 335-67.

20. Rao VG, Sarafdar RB, Chowdhury TS, Sivadas P, Yang P, et al. (2016) Myc-binding protein orthologue interacts with AKAP240 in the central pair apparatus of the Chlamydomonas flagella. BMC Cell Biol 17: 24.

21. Micsonai A, Wien F, Kernya L, Lee Y-H, Goto Y, et al. (2015) Accurate secondary structure prediction and fold recognition for circular dichroism spectroscopy. Proc Natl Acad Sci 112: E3095-E3103.

22. Xu D, Zhang Y (2012) Ab initio protein structure assembly using continuous structure fragments and optimized knowledge-based force field. Proteins 80: 1715-35.

23. Waterhouse A, Bertoni M, Bienert S, Studer G, Tauriello G, et al. (2018) SWISS-MODEL: homology modelling of protein structures and complexes. Nucleic Acids Res 46: W296-W303.

24. Benkert P, Biasini M, Schwede T (2010) Toward the estimation of the absolute quality of individual protein structure models. Bioinformatics 27: 343-50.

25. Chen VB, Arendall WB, Headd JJ, Keedy DA, Immormino RM, et al. (2010) MolProbity: all-atom structure validation for macromolecular crystallography. Acta Crystallographica Section D: Biological Crystallography 66: 12-21.

26. Kabsch W, Sander C (1983) Dictionary of protein secondary structure: pattern recognition of hydrogen-bonded and geometrical features. Biopolymers: Original Res Biomols 22: 2577-637.

27. Pettersen EF, Goddard TD, Huang CC, Couch GS, Greenblatt DM, et al. (2004) UCSF Chimera-a visualization system for exploratory research and analysis. J Comput Chem 25: 1605-12.

28. Salentin S, Schreiber S, Haupt VJ, Adasme MF, Schroeder M (2015) PLIP: fully automated protein-ligand interaction profiler. Nucl Acids Res 43: W443-W447.

29. RA Laskowski, MB Swindells (2011) LigPlot+: multiple ligand-protein interaction diagrams for drug discovery. J Chem Inf Model 51: 2778-6.

30. M. Abdalla, WA Eltayb, A. Yousif (2018) Comparison of structures among Saccharomyces cerevisiae Grxs proteins. Genes Environ 40: 17.

31. D. Nemecek, J. Stepanek, GJ Thomas (2013) Raman spectroscopy of proteins and nucleoproteins. Curr. Proto. Prot. Sci. 17.8.1-17.8.25.

32. MN Siamwiza, RC Lord, MC Chen, T. Takamatsu, I. Harada, et al. (1975) Interpretation of the doublet at 850 and 830 cm-1 in the Raman spectra of tyrosyl residues in proteins and certain model compounds. Biochem 14: 4870-6.

33. JM Benevides, P. Bondre, RL Duda, RW Hendrix, GJ Thomas (2004) Domain structures and roles in bacteriophage HK97 capsid assembly and maturation. Biochem 43: 5428-36.

34. SA Overman, GJ Thomas (1999) Raman markers of non-aromatic side chains in an α-helix assembly: Ala, Asp, Glu, Gly, Ile, Leu, Lys, Ser, and Val residues of phage fd subunits. Biochem 38: 4018-27.

35. FS Parker (1983) Applications of infrared, Raman, and resonance raman spectroscopy in biochemistry, Plenum Press, New York, , USA.

36. TG Spiro, BP Gaber (1977) Laser Raman scattering as a probe of protein structure. Ann Rev Biochem 46: 553-72.

37. SW Raso, PL Clark, C. Haase-Pettingell, J. King, GJ Thomas, Jr. (2001) Distinct cysteine sulfhydryl environments detected by analysis of Raman S-hh markers of Cys-->Ser mutant proteins. J Mol Biol 307: 899-911.

38. W. Qian, J. Bandekar, S. Krimm (1991) Vibrational analysis of crystalline tri-L-alanine. Biopolymers 31: 193-210.

39. V. Lin, J. Koenig (1976) Raman studies of bovine serum albumin. Biopolymers 15: 203-18.

40. I. Osticioli, A. Nevin, D. Anglos, A. Burnstock, S. Cather, M. Becucci, C. Fotakis, E. Castellucci (2008) Micro-Raman and fluorescence spectroscopy for the assessment of the effects of the exposure to light on films of egg white and egg yolk. J Raman Spect 39: 307-13.

41. MC Chen, RC Lord (1976) Laser-excited Raman spectroscopy of biomolecules. VIII. Conformational study of bovine serum albumin. J Am Chem Soc 98: 990-992.

42. A. Barth (2007) Infrared spectroscopy of proteins. Biochim et Biophys Acta-Bioenergetics 1767: 1073-101.

43. H. Torii, M. Tasumi, H. Mantsch, D. Chapman (1996) Infrared Spectroscopy of Biomolecules. Edited by Mantsch H. H., Chapman D., Wiley-Liss, New York, USA.

44. JT Pelton, LR McLean (2000) Spectroscopic methods for analysis of protein secondary structure. Anal. Biochem. 277: 167-76.

45. E. Goormaghtigh, J-M. Ruysschaert, V. Raussens (2006) Evaluation of the information content in infrared spectra for protein secondary structure determination. Biophys J 90: 2946-57.

46. A. Micsonai, F. Wien, É. Bulyáki, J. Kun, É. Moussong, et al. (2018) BeStSel: a web server for accurate protein secondary structure prediction and fold recognition from the circular dichroism spectra. Nuc Acids Res 46: W315-W322.

47. C. Johansson, CH Lillig, A. Holmgren (2004) Human mitochondrial glutaredoxin reduces S-glutathionylated proteins with high affinity accepting electrons from either glutathione or thioredoxin reductase. J Biol Chem 279: 7537-43.

48. C. Hsu-Han, C. Chu-Ying, C. Yu-Ting, S. Jei-Fu (2013) Novel Highly Active Recombinant Glutaredoxin from Chlorella sorokiniana T-89. J Agri Food Chem 62: 927-33.

49. C. Johansson, KL Kavanagh, O. Gileadi, U. Oppermann (2007) Reversible Sequestration of Active Site Cysteines in a 2Fe-2S-bridged Dimer Provides a Mechanism for Glutaredoxin 2 Regulation in Human Mitochondria. J Biological Chemistry 282: 3077-82.

50. R. Iversen, PA Andersen, KS Jensen, JR Winther, BW Sigurskjold (2010) Thiol– Disulfide Exchange between Glutaredoxin and Glutathione. Biochem. 49: 810-20.

51. R. Goldberg, N. Kishore, R. Lennen, (2002) CRC Handbook of Chemistry and Physics, 83rd ed. CRC Press, Boca Raton, FL, USA.

52. PD Ross, S. Subramanian (1981) Thermodynamics of protein association reactions: forces contributing to stability. Biochem 20: 3096-102.

53. G. Wu, Y-Z Fang, S. Yang, JR Lupton, ND Turner (2004) Glutathione Metabolism and its Implications for Health. J Nutr 134: 489-92.

54. AP Fernandes, M. Fladvad, C. Berndt, C. Andre´sen, CH Lillig, et al. (2005) A Novel Monothiol Glutaredoxin (Grx4) from Escherichia coli can serve as a substrate for thioredoxin reductase. J Biol Sci 280: 24544-52.

55. J. Tamarit, G. Bell, E. Cabiscol, E. Herrero, J. Ros (2003) Biochemical Characterization of Yeast Mitochondrial Grx5 Monothiol Glutaredoxin. J Biological Chemistry 278: 25745-51.

56. M. Deponte, K. Becker, S. Rahlfs (2005) Plasmodium falciparum glutaredoxin-like proteins. Biol. Chem., 386: 33-40.

57. MM Gallogly, DW Starke, AK Leonberg, SM Ospina, JJ Mieyal (2008) Kinetic and mechanistic characterization and versatile catalytic properties of mammalian glutaredoxin 2: implications for intracellular roles. Biochemistry 47: 11144-57.

58. SS Merchant, SE Prochnik, O. Vallon, EH Harris, SJ Karpowicz, et al. (2007) The Chlamydomonas Genome Reveals the Evolution of Key Animal and Plant Functions. Science 318: 245-50.

59. Collin V, Lamkemeyer P, Miginiac-Maslow M, Hirasawa M, Knaff DB, et al. (2004) Characterization of Plastidial Thioredoxins from Arabidopsis Belonging to the New y-Type. Plant Physiol. 2004; 136: 4088-4095.